Interface Charge Engineering of Ternary RuCoMo Oxide Nanofibers toward High-Current-Density Water Electrolysis

Linfeng Zhang,[a,1] Mingze Xia,[a,1] Weimo Li,*[b] Siyu Ren,[a] Li Deng,[a] Siqi Zhang,[a] Lin Huang,[a] Wei Song,[c] Xiaofeng Lu*[a]

[a]Alan G. MacDiarmid Institute, College of Chemistry Jilin University Changchun 130012, P.R. China. E-mail: xflu@jlu.edu.cn

[b]Department of Materials Science and Engineering, Zhejiang Normal University Yingbin Road 688, Jinhua 321004, P. R. China. Email: liweimo@zjnu.edu.cn

[c]State Key Laboratory of Supramolecular Structure and Materials, College of Chemistry, Jilin University, Changchun 130012, P. R. China

[1]These authors contribute equally to this work.

1. Experimental section

Chemicals. Ethanol was obtained from Sinopharm Chemical Reagent Co. Ltd. N, N-dimethylformamide (DMF) was available from Tianjin Tiantai Chemical Co., Ltd. Poly(vinylpyrrolidone) (PVP, M_w=1,300,000 g mol^{-1}) was bought from Alfa Aesar. The Bis(acetylacetonato)dioxomolybdenum(VI) ($C_{10}H_{14}MoO_6$) and cobalt nitrate hexahydrate ($Co(NO_3)\cdot 6H_2O$) were acquired from Aladdin. Nafion solution (5 wt%), ruthenium chloride ($RuCl_3\cdot xH_2O$) and commercial ruthenium oxide (RuO_2) were purchased from Sigma-Aldrich. Commercial Pt/C (20 wt%) was provided by Johnson Matthey.

Synthesis of $RuCoMoO_x$ nanofibers. $RuCoMoO_x$ nanofibers (NFs) were synthesized via electrospinning followed by calcination. Initially, 0.1 g of PVP with stoichiometrically controlled $Co(NO_3)\cdot 6H_2O$, $C_{10}H_{14}MoO_6$, and $RuCl_3\cdot xH_2O$ (total metal salt mass: 0.1 g) was dissolved in a mixed DMF/ethanol (0.7 mL/0.7 mL) solution. After stirring overnight, the solution was electrospun using a flow rate of 0.15 mL h^{-1}, an operating voltage of 16 kV, and a collection distance of 25 cm from the needle tip to

the collector. This process yields a flexible nanofibrous membrane. The as-spun membrane was calcined in air within a muffle furnace using a ramp rate of 2 °C min^{-1} to 550 °C, followed by a 2 h dwell time, producing $RuCoMoO_x$ NFs. To investigate the stoichiometric effects on catalytic performance, samples with varying molar ratios of $RuCl_3 \cdot xH_2O$, $Co(NO_3)_2 \cdot 6H_2O$ and $C_{10}H_{14}MoO_6$ (0.5:1:1, 1:1:1 and 1.5:1:1) were prepared, denoted as $0.5RuCoMoO_x$ NFs, $RuCoMoO_x$ NFs and $1.5RuCoMoO_x$ NFs, respectively. The calcined temperature was also optimized, with the resulting products designated as $RuCoMoO_x$ NFs-T, where T represents the temperature (T = 450 °C, 550 °C, 650 °C). For comparison, bare RuO_2 NFs and $CoMoO_4$ NFs were synthesized as control samples using identical procedures only without the addition of $Co(NO_3)_2 \cdot 6H_2O$/$C_{10}H_{14}MoO_6$ or $RuCl_3 \cdot xH_2O$ during electrospinning process, respectively.

Material characterizations. The morphology of the as-synthesized catalyst was characterized by field-emission scanning electron microscopy (FESEM; FEI Nova NanoSEM at 15 kV) and transmission electron microscopy (TEM; JEOL JEM-2100 at 200 kV). Further microstructural and compositional analysis utilized the FEI Tecnai G2 F20 microscope, obtaining high-resolution TEM (HRTEM) images, energy-dispersive X-ray (EDX) patterns, high-angle annular dark-field scanning TEM (HAADF-STEM) images, selected area electron diffraction (SAED) patterns, and elemental mappings. Crystal structure and valence states were examined by X-ray diffraction (XRD, PANalytical B.V. Empyrean with Cu Kα radiation) and X-ray photoelectron spectroscopy (XPS, Thermo Fisher 250xi). N_2 adsorption-desorption isotherms were obtained from AutoSorb-IQ instrument.

Electrocatalytic measurements.

Electrochemical characterizations were performed using a CHI760E workstation in 1 M KOH. A three-electrode configuration was adoped for hydrogen evolution reaction (HER) and oxygen evolution reaction (OER) assessments, with catalyst-coated carbon paper (CP, 0.09 cm^2) as the working electrode, Hg/HgO as the reference, and a graphite rod (HER) or platinum wire (OER) as the counter electrode. Catalyst ink was obtained

by dispersing 1 mg of catalyst in a mixture of 247.5 μL of ethanol, 247.5 μL of water, and 5 μL of 5 wt% Nafion solution. A 50 μL portion of this ink was applied onto the CP substrate and allowed to dry prior to testing. All potentials obtained with the Hg/HgO electrode as reference were converted to the reversible hydrogen electrode (RHE) scale following calibration in alkaline electrolyte. To ensure system stability, several cyclic voltammetry (CV) scans were conducted in Ar-saturated 1 M KOH prior to recording the data. The linear sweep voltammetry (LSV) experiments were then performed at a scan rate of 2 mV s^{-1}.

Electrochemical impedance spectroscopy (EIS) measurements were conducted at applied potentials of −1.1 V *vs.* Hg/HgO for HER and 0.65 V *vs.* Hg/HgO for OER with a frequency range from 0.1 Hz to 10^5 Hz. Double-layer capacitance (C_{dl}) values were determined from CV scans recorded at scan rates between 20 and 80 mV s^{-1} within a potential window of −0.5 to −0.4 V *vs.* Hg/HgO electrode.

The electrochemically active surface area (ECSA), derived from the C_{dl} value based on their linear relationship, was calculated using the following equation (1):

$$ECSA = C_{dl}/C_s \quad (1)$$

Roughness factor (RF) was also calculated by formula (2):

$$RF = ECSA/S \quad (2)$$

The mass $activity_{Ru}$ was calculated by formula (3):

$$Mass\ activity_{Ru}\ (MA_{Ru}) = j \times S/m_{Ru} \quad (3)$$

Turnover frequency per-Ru site (TOF_{Ru}) value was calculated by formula (4):

$$TOF_{Ru} = j \times S/(z \times F \times n_{Ru}) \quad (4)$$

The m_{Ru} and n_{Ru} are calculated based on the theoretical feed content.

The Faraday efficiency was calculated by formula (5):

$$Faraday\ efficiency = \left[z \times F \times n_{gas}/(I \times t)\right] \times 100\% \quad (5)$$

where C_s denotes the specific capacitance for a 1 cm^2 flat surface (0.04 mF cm^{-2}); S represents the surface area covered by catalysts; j indicates the current density; m_{Ru} is

the mass of Ru in different catalysts; z signifies the electrons accepted or donated for each H_2 or O_2 molecule generation (2 for HER and 4 for OER); F is the Faraday constant (96485.3 C mol^{-1}); n_{Ru} is the moles of Ru atoms in different catalysts; n_{gas} is the moles of gas evolved, and I denotes the constant current (A) applied over t (s). All the mentioned electrochemical results were corrected for *iR* compensation.

The overall water splitting (OWS) performances of the assembled alkaline electrolyzers were assessed using a two-electrode configuration. Linear sweep voltammetry (LSV) was conducted at a scan rate of 1 mV s^{-1}. Faraday efficiency was determined at 100 mA cm^{-2} by collecting the evolved gases via the water displacement method. The moles of gas produced were calculated using the ideal gas law, adopting a standard molar volume (V_m) of 24.5 L mol^{-1} at ambient temperature. All the durability tests were performed by using nickel foam as the substrate with a catalyst loading of 2 mg cm^{-2}.

DFT calculations. We performed all density functional theory (DFT) calculations using the Vienna Ab Initio Simulation Package (VASP) with the generalized gradient approximation (GGA) and the Perdew-Burke-Ernzerhof (PBE) exchange-correlation functional. The projector-augmented wave (PAW) method with a plane-wave basis set was employed. An energy cutoff of 520 eV was applied for the plane-wave basis set. Brillouin zone sampling used Monkhorst-Pack grids: a 3×3×3 grid for bulk materials and a 3×3×1 grid for slab models. Geometry optimization and self-consistent field calculations were performed using these settings. The convergence criteria for both material types were set to an energy change below 10^{-7} eV between electronic steps and forces on each atom below 0.03 eV $Å^{-1}$. The Gibbs free energy(ΔG) was calculated by using the formula (6)

$$\Delta G = \Delta E + \Delta E_{ZPE} - T\Delta S \quad (6)$$

where ΔE_{ZPE} denotes the zero-point energy correction and ΔS represents the entropy change of intermediate species.[1,2]

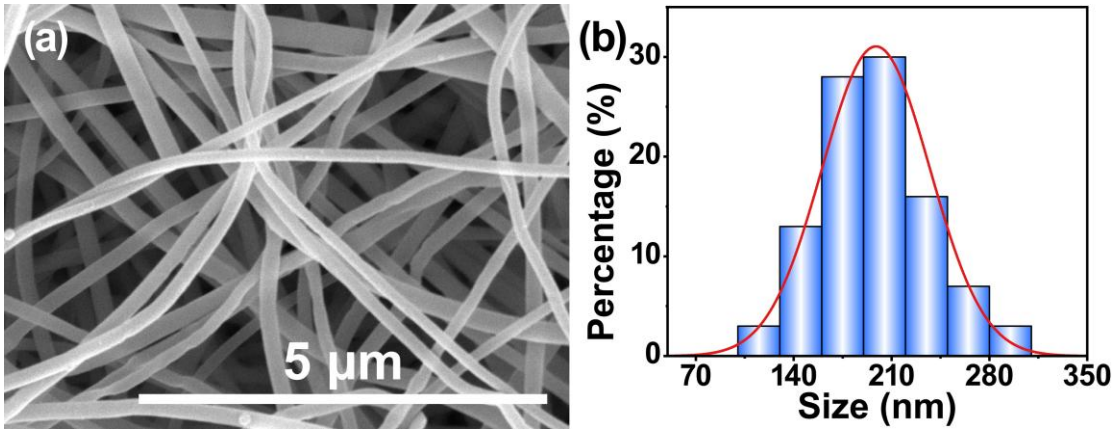

Fig. S1. (a) SEM image and (b) size distribution histogram of precursor NFs.

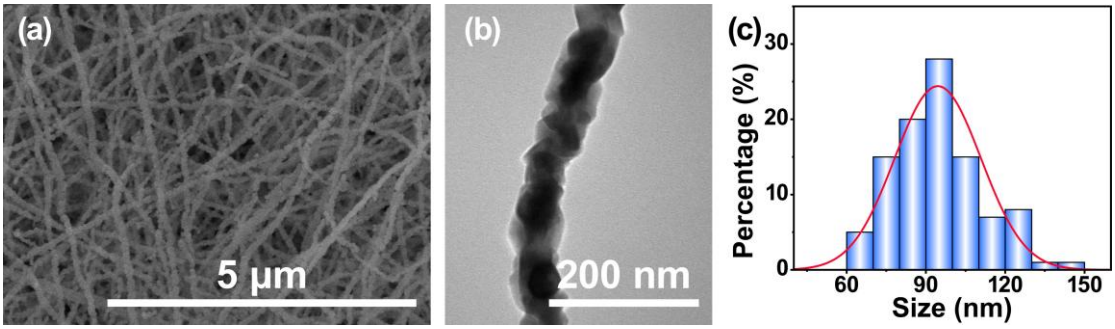

Fig. S2. (a) SEM image, (b) TEM image, and (c) size distribution histogram of $CoMoO_4$ NFs.

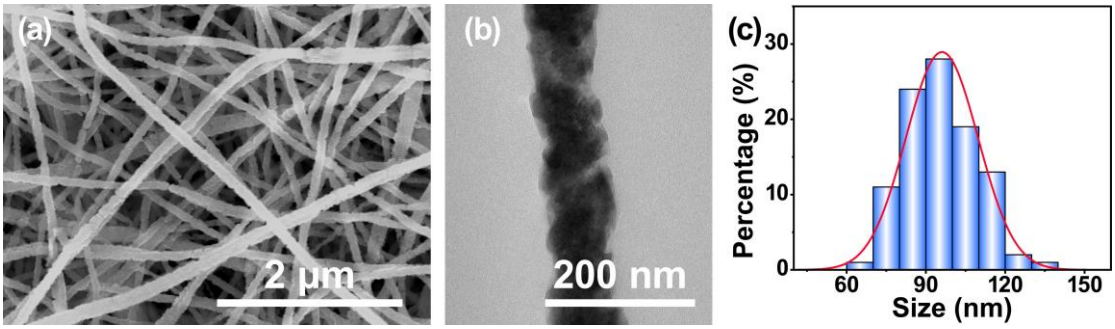

Fig. S3. (a) SEM image, (b) TEM image, and (c) size distribution histogram of $0.5RuCoMoO_x$ NFs.

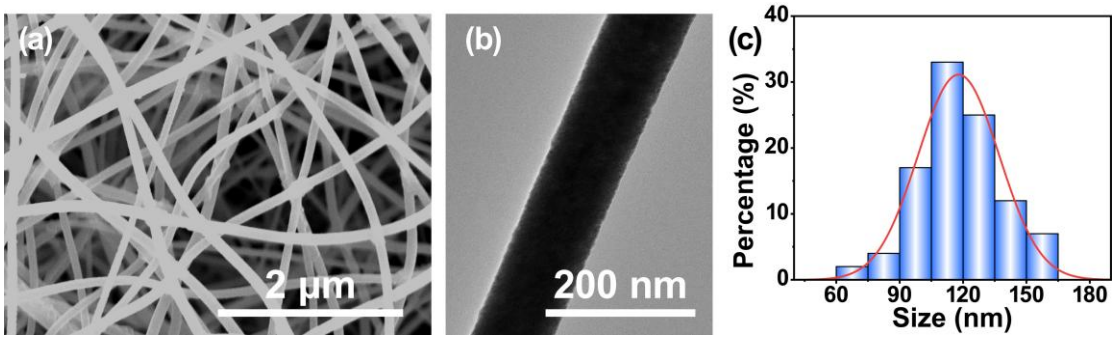

Fig. S4. (a) SEM image, (b) TEM image, and (c) size distribution histogram of 1.5RuCoMoO_x NFs.

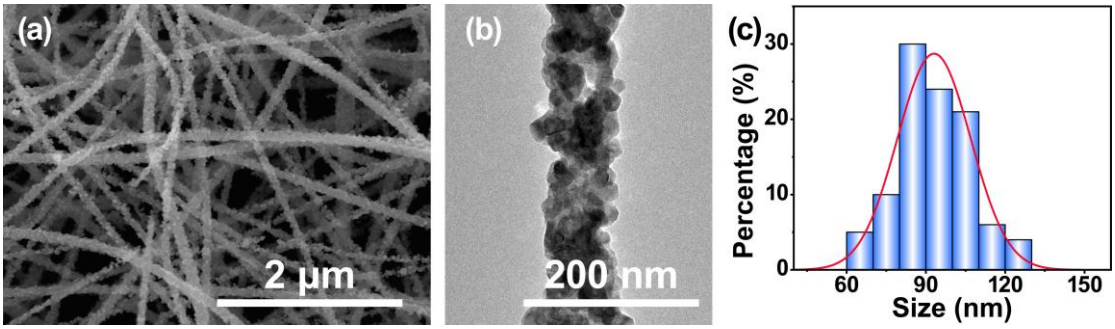

Fig. S5. (a) SEM image, (b) TEM image, and (c) size distribution histogram of RuO_2 NFs.

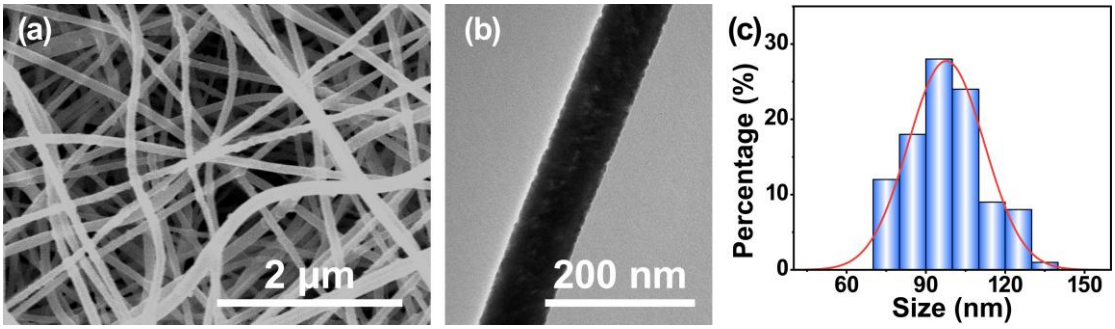

Fig. S6. (a) SEM image, (b) TEM image, and (c) size distribution histogram of $RuCoMoO_x$ NFs-450.

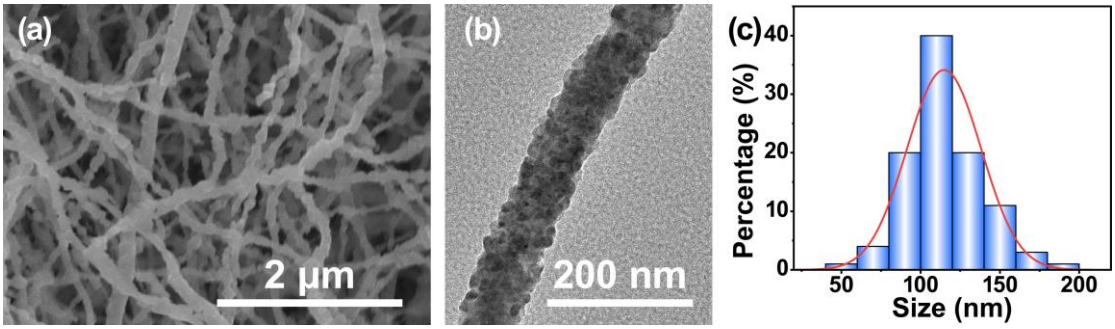

Fig. S7. (a) SEM image, (b) TEM image, and (c) size distribution histogram of $RuCoMoO_x$ NFs-650.

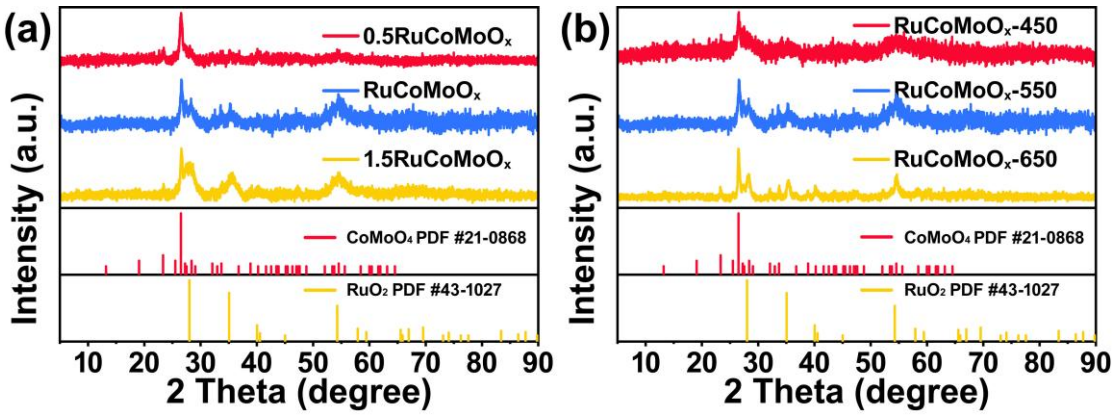

Fig. S8. XRD patterns of (a) $xRuCoMoO_x$ NFs with different RuO_2:$CoMoO_4$ ratios (x = 0.5, 1, 1.5) and (b) $RuCoMoO_x$ NFs -T calcined at different temperatures (T = 450 °C, 550 °C, 650 °C).

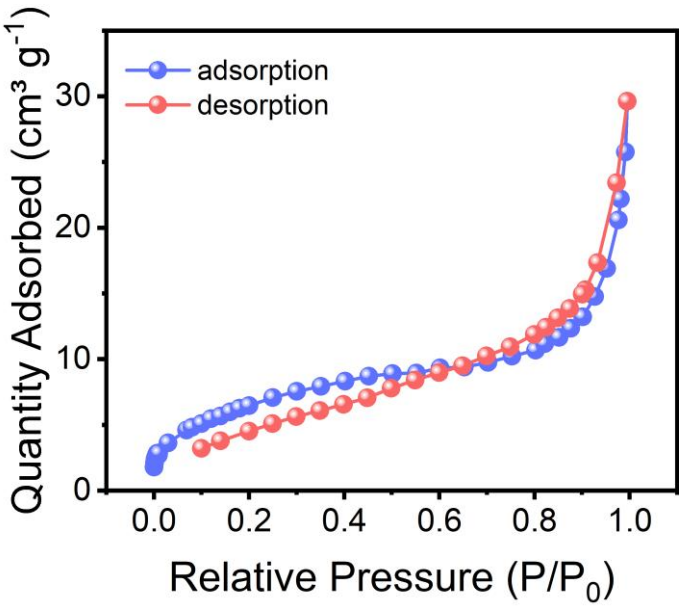

Fig. S9. The N_2 adsorption-desorption isotherms of $RuCoMoO_x$ NFs.

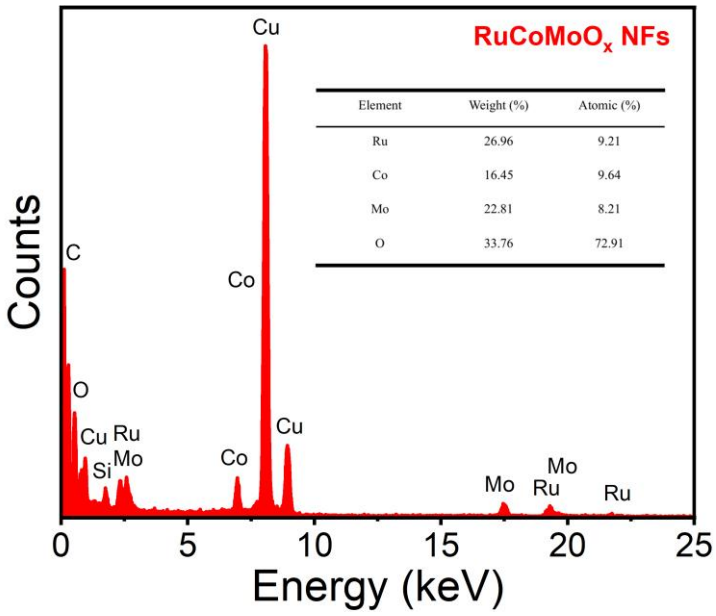

Fig. S10. EDX spectrum of $RuCoMoO_x$ NFs.

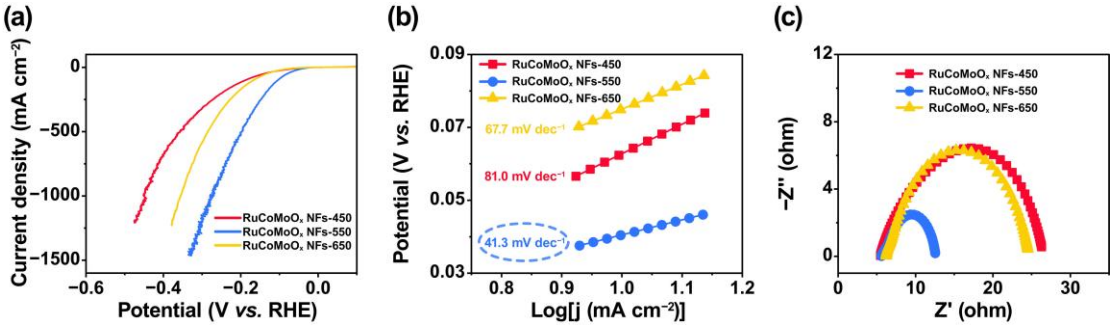

Fig. S11. (a) LSV curves, (b) Tafel slopes, and (c) Nyquist plots of $RuCoMoO_x$ NFs-T calcined at different temperatures (T = 450 °C, 550 °C, 650 °C) for HER.

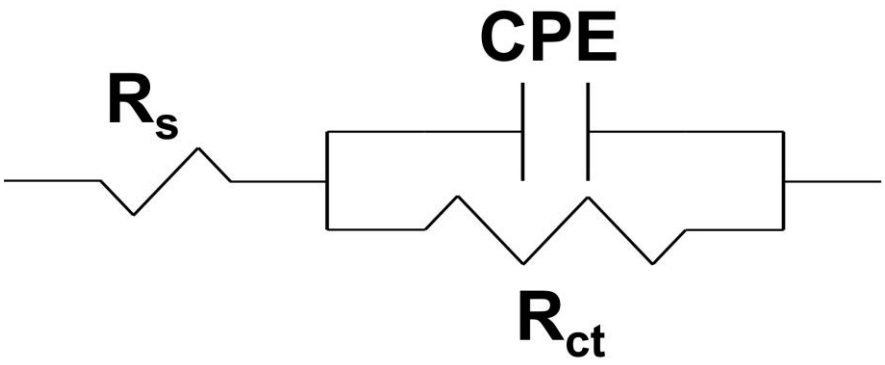

Fig. S12. The equivalent circuit model used for simulating the Nyquist plots in 1 M KOH solution.

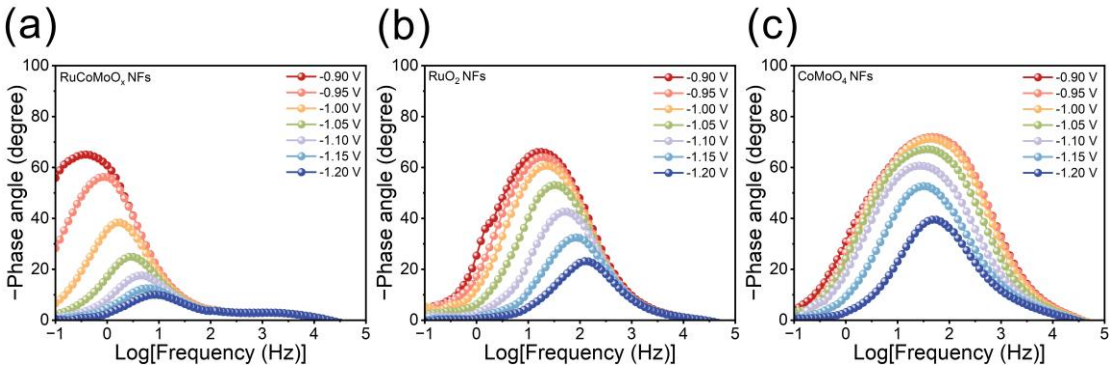

Fig. S13. The Bode phase plots at different voltages for (a) $RuCoMoO_x$ NFs, (b) RuO_2 NFs, and (c) $CoMoO_4$ NFs toward HER (The potential shown in the figures is relative to the Hg/HgO reference electrode.).

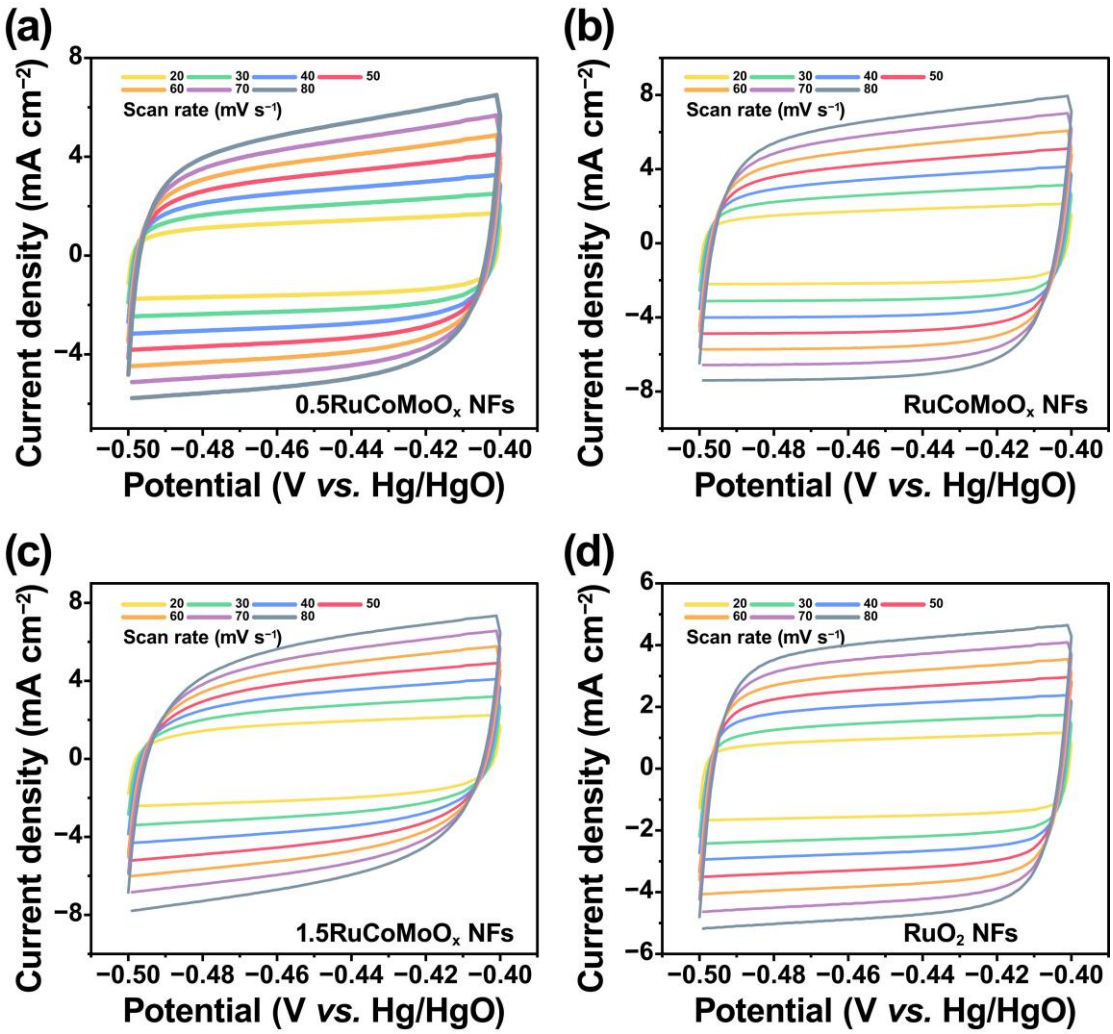

Fig. S14. CV curves at various scan rates for (a) 0.5RuCoMoO$_x$ NFs, (b) RuCoMoO$_x$ NFs, (c) 1.5RuCoMoO$_x$ NFs, and (d) RuO$_2$ NFs.

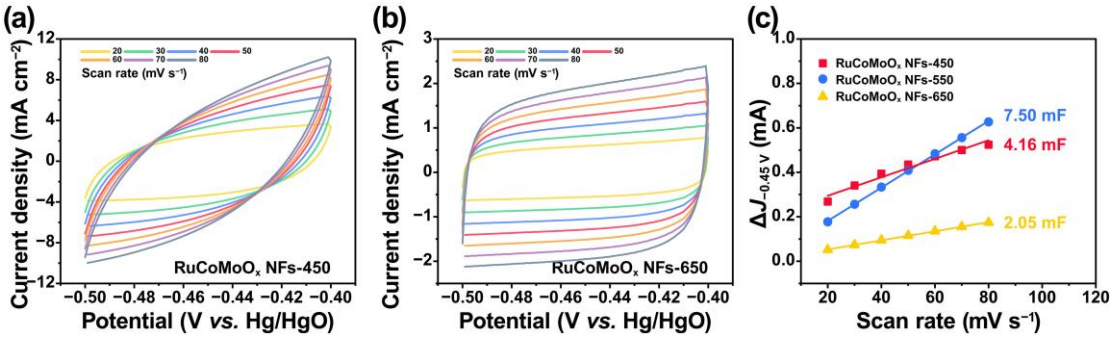

Fig. S15. CV curves at various scan rates of $RuCoMoO_x$ NFs calcined at (a) 450 °C and (b) 650 °C. (c) Corresponding double-layer capacitance (C_{dl}).

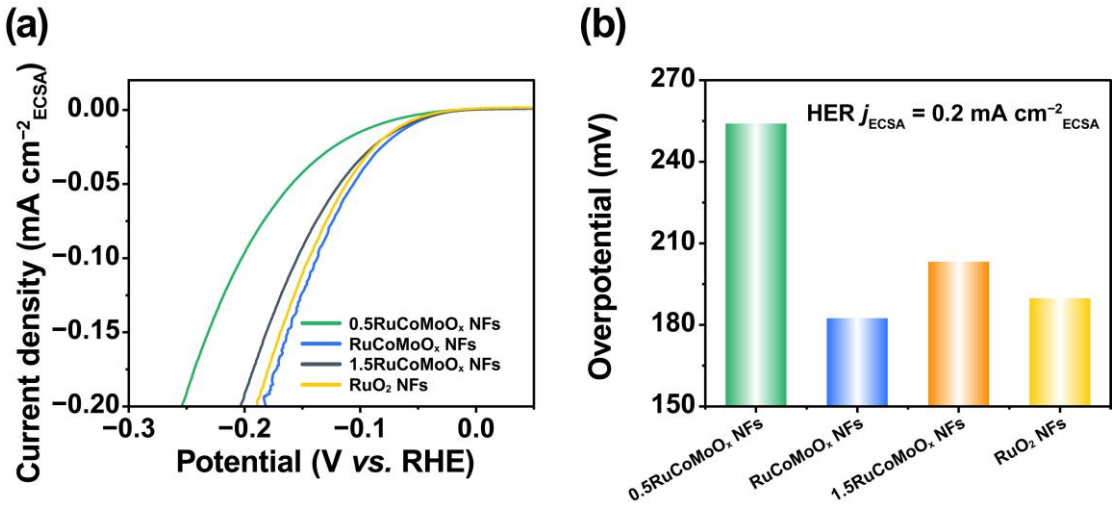

Fig. S16. (a) Normalized HER polarization curves and (b) corresponding overpotentials at 0.2 mA cm^{-2} derived from normalized curves for $RuCoMoO_x$ NFs and control samples.

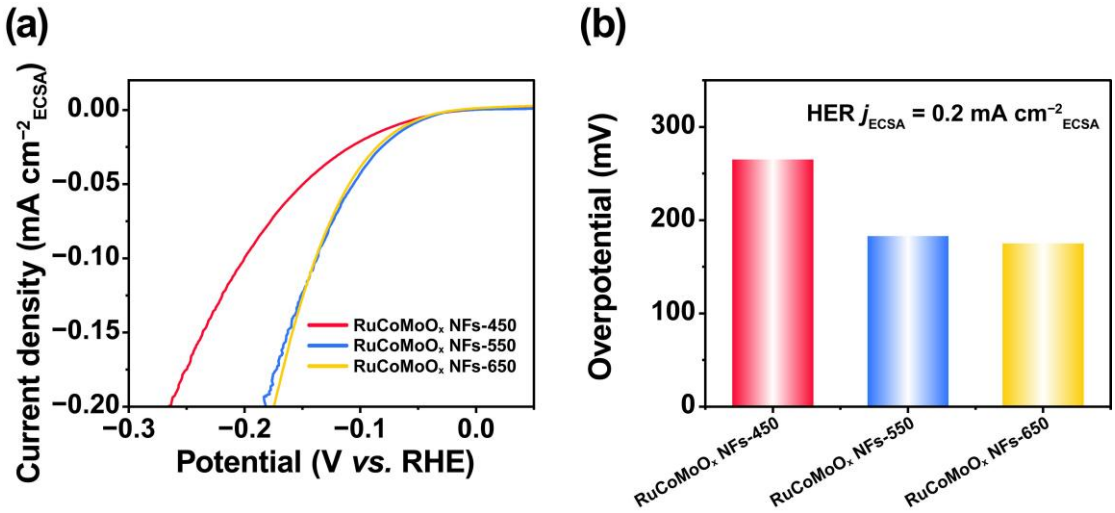

Fig. S17. (a) Normalized HER polarization curves and (b) corresponding overpotentials at 0.2 mA cm^{-2} derived from normalized curves for RuCoMoO$_x$ NFs and control samples calcined at different temperatures.

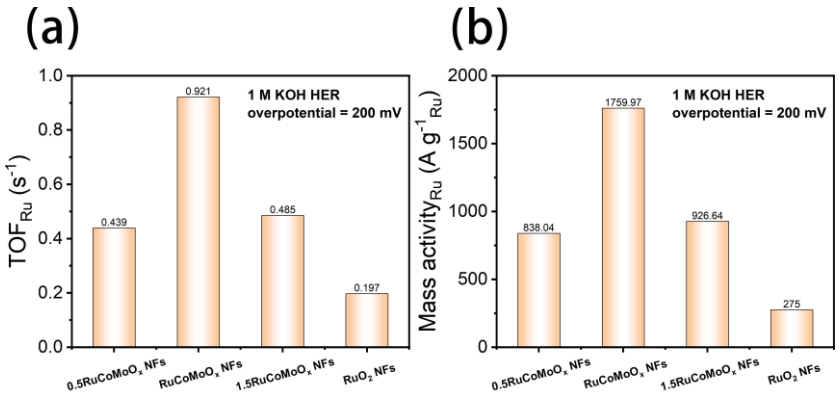

Fig. S18. (a) TOF and (b) mass activity values of $RuCoMoO_x$ NFs and control samples for HER.

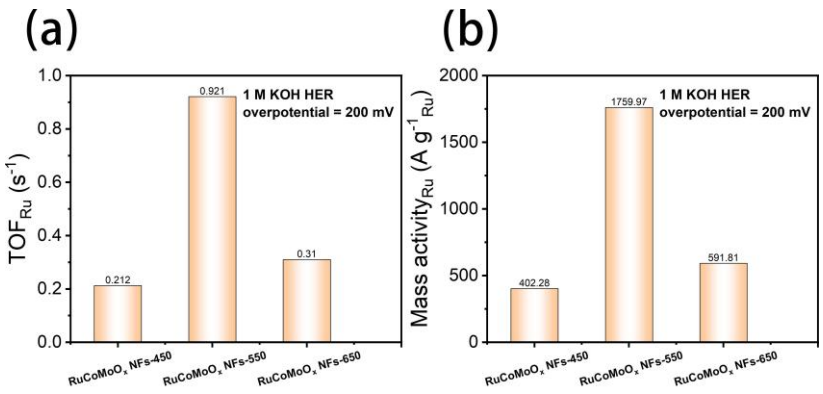

Fig. S19. (a) TOF and (b) mass activity values of $RuCoMoO_x$ NFs and control samples calcined at different temperatures for HER.

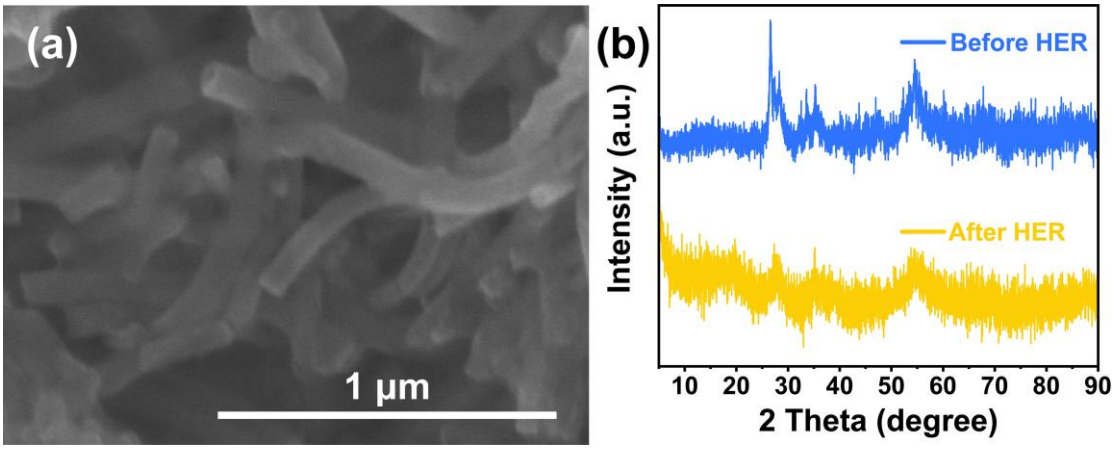

Fig. S20. (a) SEM image of $RuCoMoO_x$ NFs after HER stability test. (b) XRD patterns of $RuCoMoO_x$ NFs before and after HER stability test.

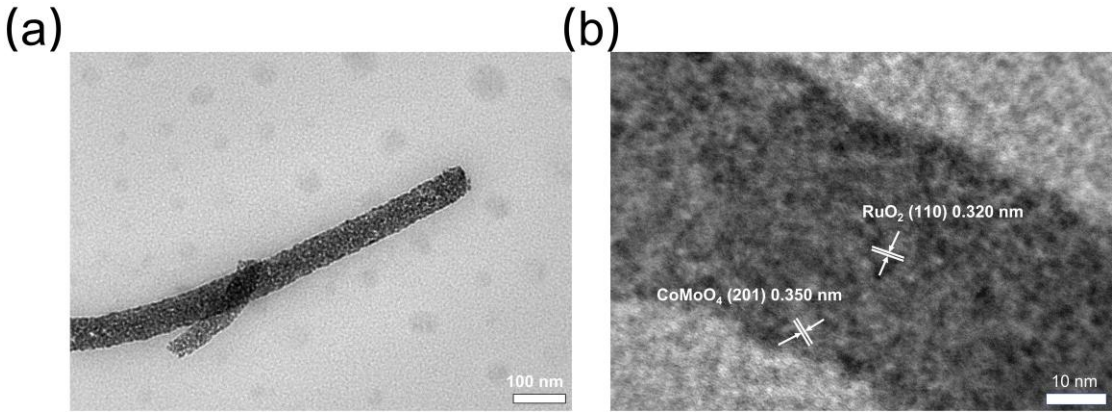

Fig. S21. (a) TEM and (b) HRTEM images of $RuCoMoO_x$ NFs after HER stability test.

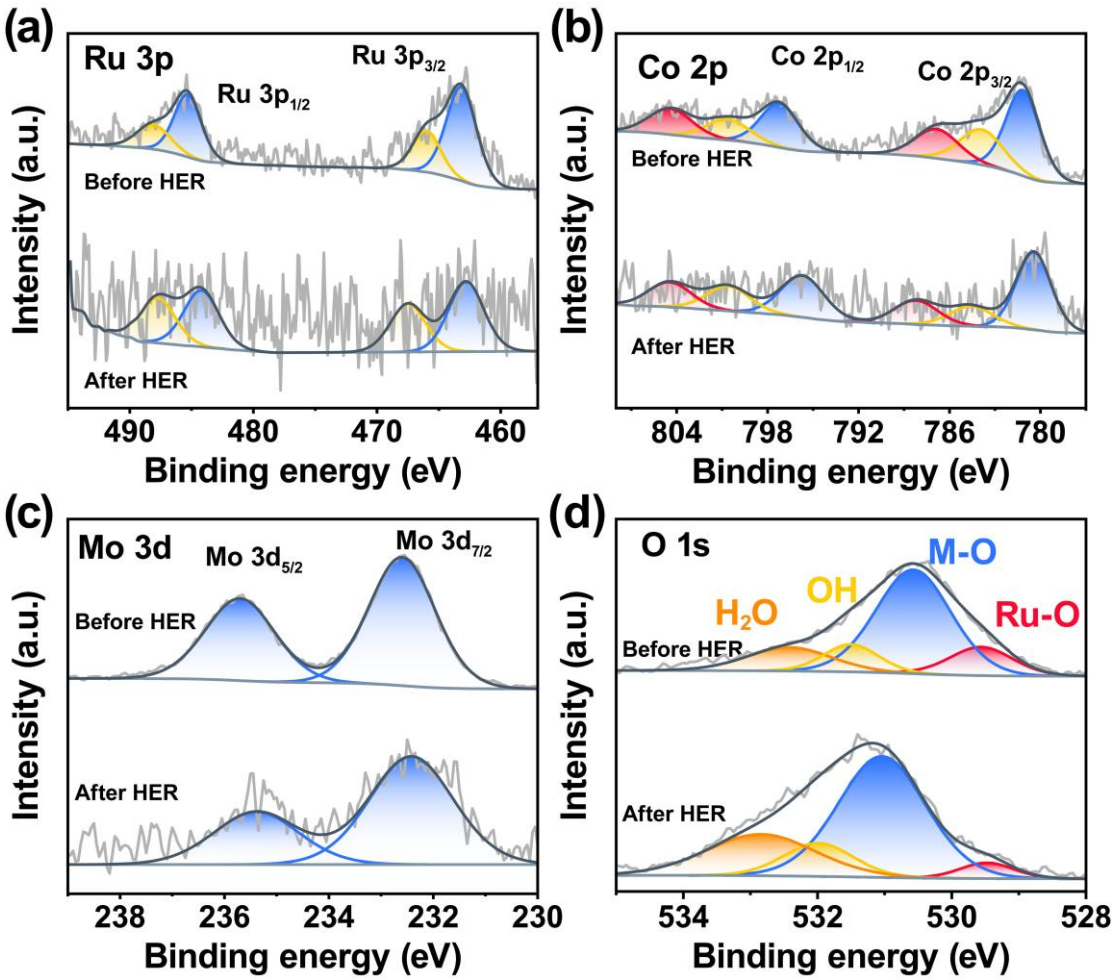

Fig. S22. (a) Ru 3p, (b) Co 2p, (c) Mo 3d, and (d) O 1s XPS spectra of $RuCoMoO_x$ NFs before and after HER stability test.

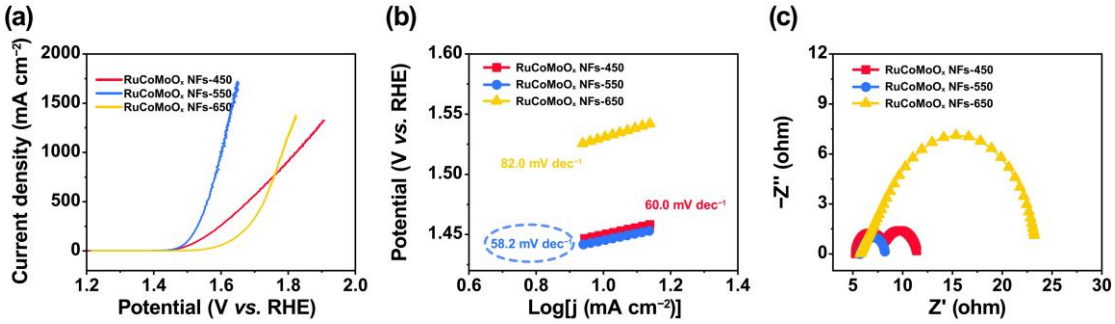

Fig. S23. (a) LSV curves, (b) Tafel slopes, and (c) Nyquist plots of $RuCoMoO_x$ NFs-T calcined at different temperatures (T = 450 °C, 550 °C, 650 °C) for OER.

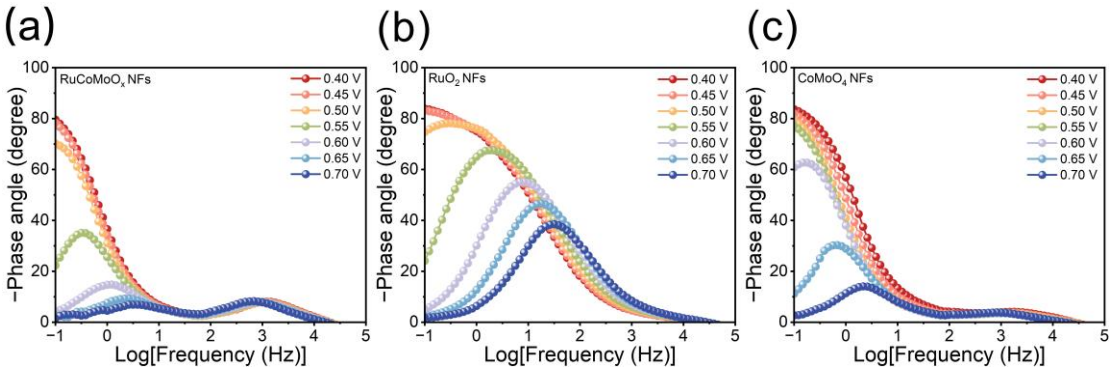

Fig. S24. The Bode phase plots at different voltages for (a) $RuCoMoO_x$ NFs, (b) RuO_2 NFs, and (c) $CoMoO_4$ NFs toward OER (The potential shown in the figures is relative to the Hg/HgO reference electrode).

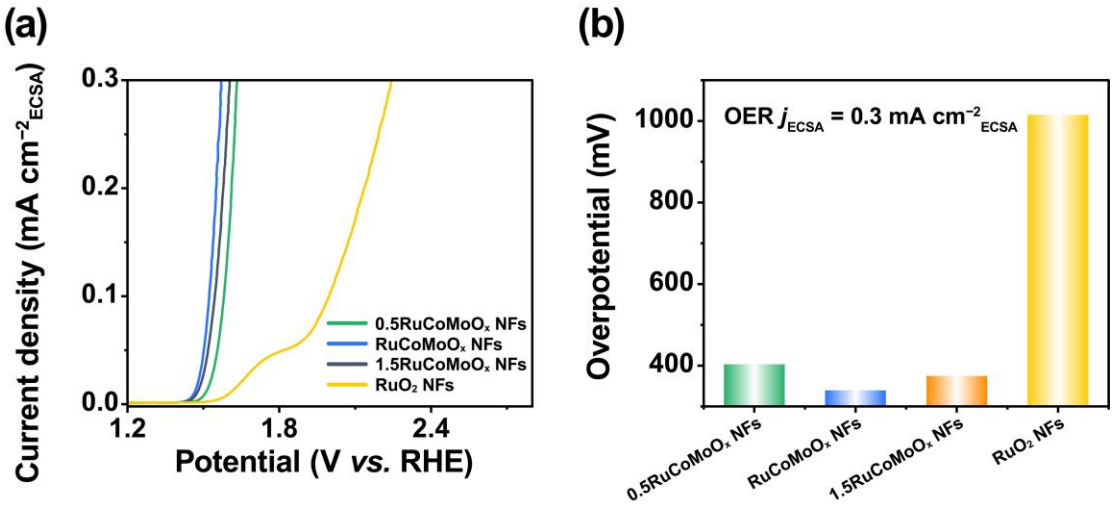

Fig. S25. (a) Normalized OER polarization curves and (b) corresponding overpotentials at 0.3 mA cm$^{-2}_{ECSA}$ derived from normalized curves for RuCoMoO$_x$ NFs and control samples.

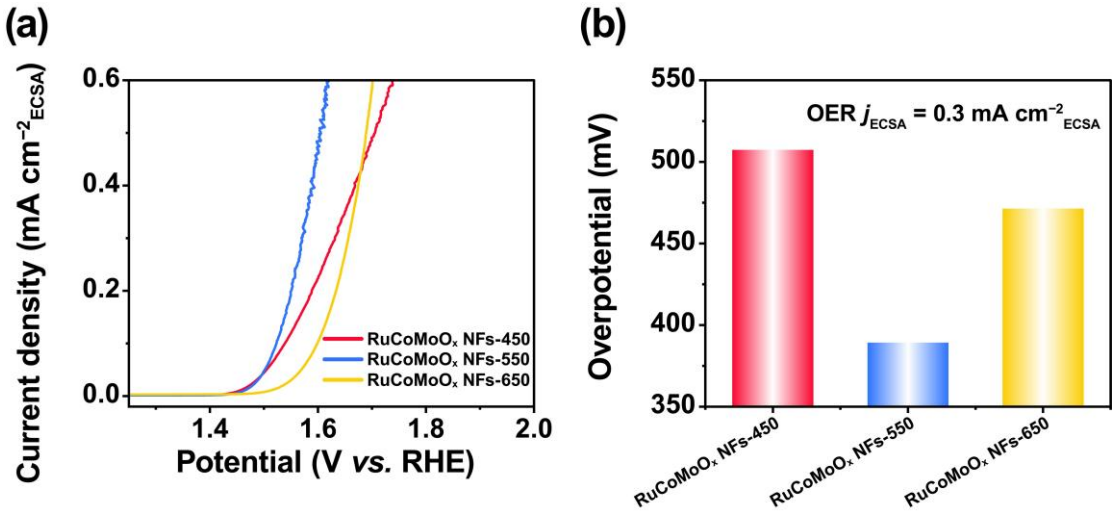

Fig. S26. (a) Normalized OER polarization curves and (b) corresponding overpotentials at 0.3 mA cm^{-2}_{ECSA} derived from normalized curves for $RuCoMoO_x$ NFs and control samples calcined at different temperatures.

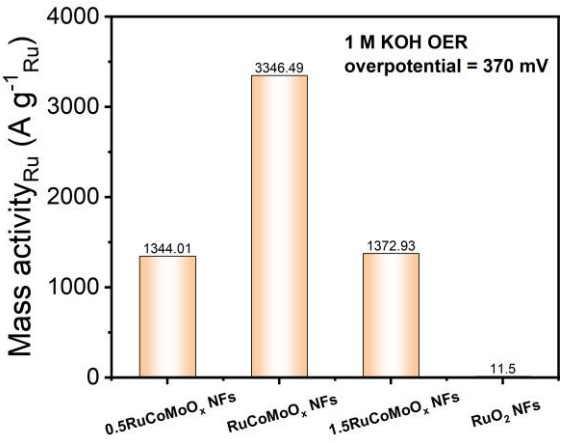

Fig. S27. Mass activity values of $RuCoMoO_x$ NFs and control samples for OER.

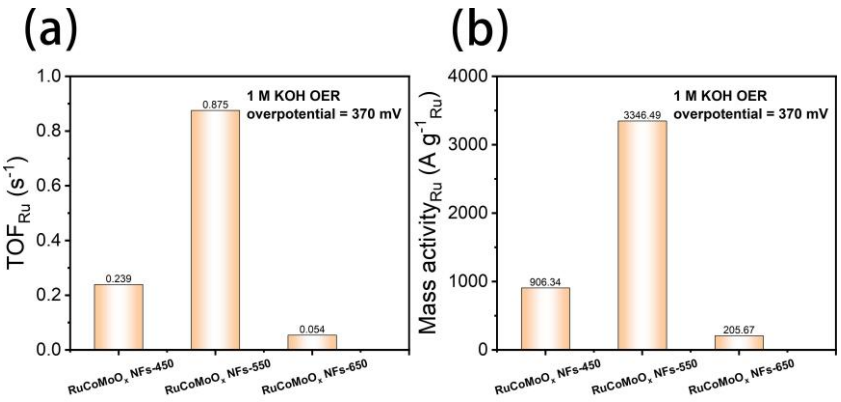

Fig. S28. (a) TOF and (b) mass activity values of $RuCoMoO_x$ NFs and control samples calcined at different temperatures for OER.

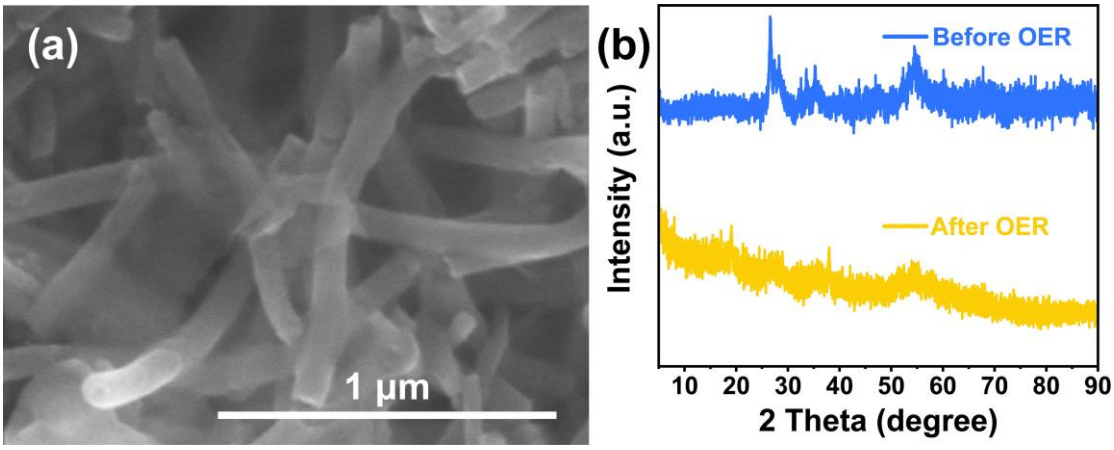

Fig. S29. (a) SEM image of $RuCoMoO_x$ NFs after OER stability test. (b) XRD patterns of $RuCoMoO_x$ NFs before and after OER stability test.

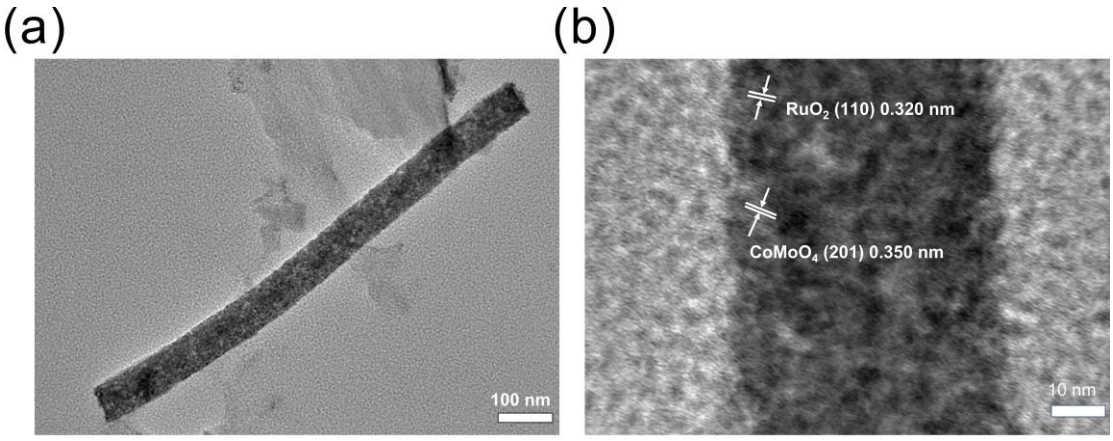

Fig. S30. (a) TEM and (b) HRTEM images of $RuCoMoO_x$ NFs after OER stability test.

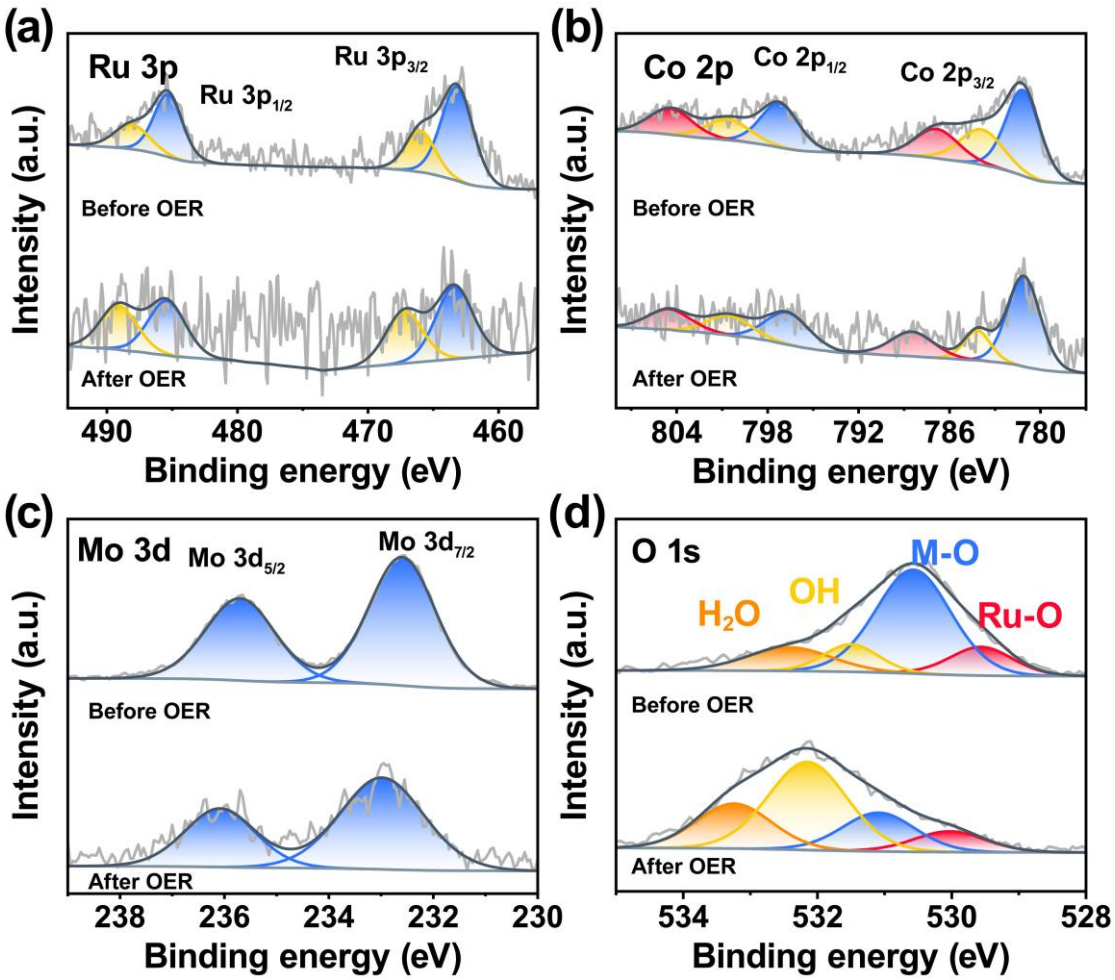

Fig. S31. (a) Ru 3p, (b) Co 2p, (c) Mo 3d, and (d) O 1s XPS spectra of $RuCoMoO_x$ NFs before and after OER stability testing.

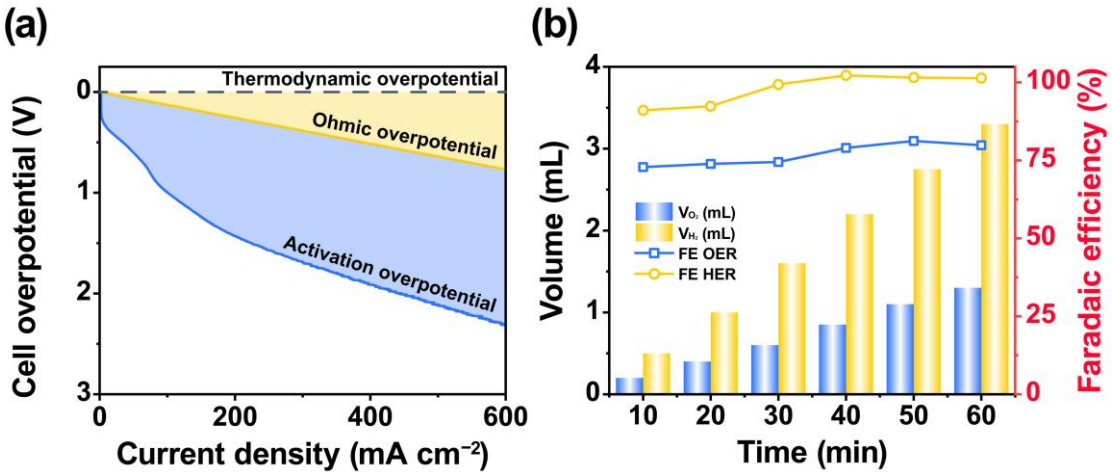

Fig. S32. (a) Contributions of ohmic overpotential and activation overpotential and (b) Faradaic efficiency of commercial Pt/C||commercial RuO_2.

Table S1 Comparisons of $RuCoMoO_x$ NFs with other reported catalysts for HER in 1 M KOH.

Catalysts	Electrolyte	J (mA cm^{-2})	η (mV)	Tafel slope (mV dec^{-1})	References
$RuCoMoO_x$ NFs	1.0 M KOH	10	40.9	41.3	This work
		100	105		
		1000	275		
$CuS@MoSe_2$	1.0 M KOH	10	72	148.8	[3]
Cu-Ni_3S_2/Co_3S_4	1.0 M KOH	10	79	50.4	[4]
Ru-Cu	1.0 M KOH	10	62	37	[5]
$PdHCu_{11}$	1.0 M KOH	10	50	80	[6]
$NiMoP_x@Ni_5P_4$	1.0 M KOH	10	101	100.7	[7]
Cu,Co/NSC1	1.0 M KOH	10	159	75.9	[8]
H-Mo_2C/NG	1.0 M KOH	10	63	48	[9]
Ni_{SA}-O/Mo_2C	1.0 M KOH	10	133	89.36	[10]
A-NiCo LDH/NF	1.0 M KOH	1000	381	57	[11]
$NiCoS_xSe_y$	1.0 M KOH	1000	345	34	[12]
N-NiMoS	1.0 M KOH	1000	322	86	[13]
Sn-$Ni(OH)_2$	1.0 M KOH	1000	550	65.5	[14]
Co-Mo_5N_6	1.0 M KOH	1000	280	29.0	[15]
$NiCo_{(nf)}$-P	1.0 M KOH	1000	317	112	[16]
CoP_3-Nb_2P/PCC	1.0 M KOH	1000	375	72.8	[17]
NC@CrN/Ni	1.0 M KOH	1000	284	40	[18]
FeIr/NF	1.0 M KOH	1000	327	64.78	[19]
Ru-FeP_4/IF	1.0 M KOH	1000	296	51.58	[20]
F,P-Fe_3O_4	1.0 M KOH	1000	321.3	127.9	[21]
$NiCoS_x$@CoCH NAs/NF	1.0 M KOH	1000	438.5	107.8	[22]

Table S2 C_{dl}, ECSA and RF values of $RuCoMoO_x$ NFs with other catalysts.

Catalysts	C_{dl} (mF)	ECSA (cm^2)	RF
0.5$RuCoMoO_x$ NFs	5.51	137.925	1532.5
$RuCoMoO_x$ NFs	7.50	187.425	2082.5
1.5$RuCoMoO_x$ NFs	6.28	157.05	1745
RuO_2 NFs	4.78	119.475	1327.5
$RuCoMoO_x$-450 NFs	4.16	104.175	1157.5
$RuCoMoO_x$-650 NFs	2.05	51.075	567.5

Table S3 Comparisons of $RuCoMoO_x$ NFs with other reported catalysts for OER in 1 M KOH.

Catalysts	Electrolyte	J (mA cm^{-2})	η (mV)	Tafel slope (mV dec^{-1})	References
$RuCoMoO_x$ NFs	1.0 M KOH	10	231	58.2	This work
		100	293		
		1000	368		
S|NiN_x–PC/EG	1.0 M KOH	10	280	45	[23]
a/c-NiFe-G	1.0 M KOH	10	217	33.9	[24]
Ni SAs@S/N-CMF	1.0 M KOH	10	285	50.8	[25]
RuO_2/CoO_x	1.0 M KOH	10	240	70	[26]
NiFe-*S*-TCNQ	1.0 M KOH	10	209	36.1	[27]
NiTe/NiS	1.0 M KOH	100	257	49	[28]
Fe,V co-doped NiOOH	1.0 M KOH	100	264	39	[29]
Au_{SA}-MnFeCoNiCu	1.0 M KOH	10	213	27.5	[30]
Se-doped FeOOH	1.0 M KOH	10	287	54	[31]
FeMnS/FeMnP/NF	1.0 M KOH	1000	374	65.9	[32]
VOs-Co_3O_4/CoO NWs@Cu@NF	1.0 M KOH	1000	391	56.8	[33]
c-FeOOH/ α -$Ni(OH)_2$/NF	1.0 M KOH	1000	390	51.4	[34]
Ni-Fe-OH@Ni_3S_2/NF	1.0 M KOH	1000	469	93	[35]
Fe_2O_3@Ni_2P/$Ni(PO_3)_2$/NF	1.0 M KOH	1000	370	48.2	[36]
P-NiCoV-LTH	1.0 M KOH	1000	373	68.61	[37]
Co_1Mn_1CH/NF	1.0 M KOH	1000	462	N/A	[38]
NiCo@C-NiCoMoO/NF	1.0 M KOH	1000	390	75.15	[39]
Ni@C-MoO_2/NF	1.0 M KOH	1000	400	52.34	[40]
C-$Ni_{1-x}O$/3DNF	1.0 M KOH	1000	425	N/A	[41]
Ni-FeO_x/$FeNi_3$	1.0 M KOH	1000	405	103.0	[42]

Table S4 Comparisons of $RuCoMoO_x$ NFs with other reported catalysts for OWS in 1 M KOH.

Catalysts	Electrolyte	J (mA cm^{-2})	Voltage (V)	References
$RuCoMoO_x$ NFs	1.0 M KOH	10	1.53	This work
δ-FeOOH NSs/NF	1.0 M KOH	10	1.62	[43]
FeS/IF	1.0 M KOH	10	1.65	[44]
FeP	1.0 M KOH	10	1.59	[45]
OESSC	1.0 M KOH	10	1.74	[46]
Fe-N_4 SAs/NPC	1.0 M KOH	10	1.67	[47]
$Co(OH)_2$@NCNTs@NF	1.0 M KOH	10	1.72	[48]
Co_3S_4/EC-MOF	1.0 M KOH	10	1.55	[49]
Co_2P/CoNPC	1.0 M KOH	10	1.64	[50]
CoP NFs	1.0 M KOH	10	1.65	[51]
Co-NC@CC	1.0 M KOH	10	1.57	[52]
Co@N-CS/N-HCP@CC	1.0 M KOH	10	1.545	[53]
$Ni/Ni(OH)_2$	1.0 M KOH	10	1.59	[54]
NiS/G	1.0 M KOH	10	1.54	[55]
Ni-ZIF/Ni-B@NF	1.0 M KOH	10	1.54	[56]
Ni@NC	1.0 M KOH	10	1.6	[57]
Ni@N-HCGHF	1.0 M KOH	10	1.6	[58]
NiFeSe@NiSe|O@CC	1.0 M KOH	10	1.56	[59]
CoP@FeCoP	1.0 M KOH	10	1.68	[60]
$CoSn_2$	1.0 M KOH	10	1.55	[61]
Co_9S_8/Ni_3S_2	1.0 M KOH	10	1.64	[62]

References

1 K. Momma and F. Izumi, *J. Appl. Crystallogr.*, 2011, **44**, 1272–1276.

2 V. Wang, N. Xu, J.-C. Liu, G. Tang and W.-T. Geng, *Comput. Phys. Commun.*, 2021, **267**, 108033.

3 M. Gu, L. Jiang, S. Zhao, H. Wang, M. Lin, X. Deng, X. Huang, A. Gao, X. Liu, P. Sun and X. Zhang, *ACS Nano*, 2022, **16**, 15425–15439.

4 H. Su, S. Song, S. Li, Y. Gao, L. Ge, W. Song, T. Ma and J. Liu, *Appl. Catal., B*, 2021, **293**, 120225.

5 H. Huang, H. Jung, S. Li, S. Kim, J. W. Han and J. Lee, *Nano Energy*, 2022, **92**, 106763.

6 R. P. Brocha Silalahi, Y. Jo, J. Liao, T. Chiu, E. Park, W. Choi, H. Liang, S. Kahlal, J. Saillard, D. Lee and C. W. Liu, *Angew. Chem. Int. Ed.*, 2023, **62**, e202301272.

7 B. Zhu, J. Xiong, S. Wu, K. You, B. Sun, Y. Liu, M. Chen, P. Jin and L. Feng, *Adv. Funct. Mater.*, 2024, **34**, 2407236.

8 Y. Chen, J. Mao, H. Zhou, L. Xing, S. Qiao, J. Yuan, B. Mei, Z. Wei, S. Zhao, Y. Tang and C. Liu, *Adv. Funct. Mater.*, 2024, **34**, 2311664.

9 Y. Yang, Y. Qian, Z. Luo, H. Li, L. Chen, X. Cao, S. Wei, B. Zhou, Z. Zhang, S. Chen, W. Yan, J. Dong, L. Song, W. Zhang, R. Feng, J. Zhou, K. Du, X. Li, X.-M. Zhang and X. Fan, *Nat. Commun.*, 2022, **13**, 7225.

10 M. Hou, L. Zheng, D. Zhao, X. Tan, W. Feng, J. Fu, T. Wei, M. Cao, J. Zhang and C. Chen, *Nat. Commun.*, 2024, **15**, 1342.

11 H. Yang, Z. Chen, P. Guo, B. Fei and R. Wu, *Appl. Catal., B*, 2020, **261**, 118240.

12 S. Ma, J. Huang, C. Zhang, G. Chen, W. Chen, T. Shao, T. Li, X. Zhang, T. Gong and K. K. Ostrikov, *Chem. Eng. J.*, 2022, **435**, 134859.

13 C. Huang, L. Yu, W. Zhang, Q. Xiao, J. Zhou, Y. Zhang, P. An, J. Zhang and Y. Yu, *Appl. Catal., B*, 2020, **276**, 119137.

14 J. Jian, X. Kou, H. Wang, L. Chang, L. Zhang, S. Gao, Y. Xu and H. Yuan, *ACS Appl. Mater. Interfaces*, 2021, **13**, 42861–42869.

15 F. Lin, Z. Dong, Y. Yao, L. Yang, F. Fang and L. Jiao, *Adv. Energy Mater.*, 2020,

10, 2002176.

16 Z. Xu, C.-L. Yeh, J.-L. Chen, J. T. Lin, K.-C. Ho and R. Y.-Y. Lin, *ACS Sustainable Chem. Eng.*, 2022, **10**, 11577–11586.

17 H. Xiang, W. Chen, T. Li, J. Huang, G. Chen, T. Gong and K. Ken Ostrikov, *Chem. Eng. J.*, 2022, **446**, 137419.

18 Z. Sun, B. Chu, S. Wang, L. Dong, Q. Pang, M. Fan, X. Zhang, H. He, B. Li and Z. Chen, *J. Colloid Interface Sci.*, 2023, **646**, 361–369.

19 J. Chen, Y. Wang, G. Qian, T. Yu, Z. Wang, L. Luo, F. Shen and S. Yin, *Chem. Eng. J.*, 2021, **421**, 129892.

20 T. Cui, J. Chi, J. Zhu, X. Sun, J. Lai, Z. Li and L. Wang, *Appl. Catal., B*, 2022, **319**, 121950.

21 X.-Y. Zhang, F.-T. Li, R.-Y. Fan, J. Zhao, B. Dong, F.-L. Wang, H.-J. Liu, J.-F. Yu, C.-G. Liu and Y.-M. Chai, *J. Mater. Chem. A*, 2021, **9**, 15836–15845.

22 X. Zhang, R. Zheng, M. Jin, R. Shi, Z. Ai, A. Amini, Q. Lian, C. Cheng and S. Song, *ACS Appl. Mater. Interfaces*, 2021, **13**, 35647–35656.

23 Y. Hou, M. Qiu, M. G. Kim, P. Liu, G. Nam, T. Zhang, X. Zhuang, B. Yang, J. Cho, M. Chen, C. Yuan, L. Lei and X. Feng, *Nat. Commun.*, 2019, **10**, 1392.

24 Z. Gong, R. Liu, H. Gong, G. Ye, J. Liu, J. Dong, J. Liao, M. Yan, J. Liu, K. Huang, L. Xing, J. Liang, Y. He and H. Fei, *ACS Catal.*, 2021, **11**, 12284–12292.

25 Y. Zhao, Y. Guo, X. F. Lu, D. Luan, X. Gu and X. W. (David) Lou, *Adv. Mater.*, 2022, **34**, 2203442.

26 K. Du, L. Zhang, J. Shan, J. Guo, J. Mao, C.-C. Yang, C.-H. Wang, Z. Hu and T. Ling, *Nat. Commun.*, 2022, **13**, 5448.

27 Y. Lin, J. Fang, W. Wang, Q. Wen, D. Huang, D. Ding, Z. Li, Y. Liu, Y. Shen and T. Zhai, *Adv. Energy Mater.*, 2023, **13**, 2300604.

28 Z. Xue, X. Li, Q. Liu, M. Cai, K. Liu, M. Liu, Z. Ke, X. Liu and G. Li, *Adv. Mater.*, 2019, **31**, 1900430.

29 J. Jiang, F. Sun, S. Zhou, W. Hu, H. Zhang, J. Dong, Z. Jiang, J. Zhao, J. Li, W. Yan and M. Wang, *Nat. Commun.*, 2018, **9**, 2885.

30 F. Wang, P. Zou, Y. Zhang, W. Pan, Y. Li, L. Liang, C. Chen, H. Liu and S. Zheng, *Nat. Commun.*, 2023, **14**, 6019.

31 S. Niu, W.-J. Jiang, Z. Wei, T. Tang, J. Ma, J.-S. Hu and L.-J. Wan, *J. Am. Chem. Soc.*, 2019, **141**, 7005–7013.

32 J. Wang, Y. Zhang, W. Zhang, Q. Zhao, J. Li and G. Liu, *Electrochim. Acta*, 2023, **438**, 141563.

33 T. Liu, A. Li, W. Zhou and C. Lyu, *Chem. Eng. J.*, 2021, **415**, 128941.

34 X. Cheng, J. Yuan, J. Cao, C. Lei, B. Yang, Z. Li, X. Zhang, C. Yuan, L. Lei and Y. Hou, *J. Colloid Interface Sci.*, 2020, **579**, 340–346.

35 X. Zou, Y. Liu, G. Li, Y. Wu, D. Liu, W. Li, H. Li, D. Wang, Y. Zhang and X. Zou, *Adv. Mater.*, 2017, **29**, 1700404.

36 X. Cheng, Z. Pan, C. Lei, Y. Jin, B. Yang, Z. Li, X. Zhang, L. Lei, C. Yuan and Y. Hou, *J. Mater. Chem. A*, 2019, **7**, 965–971.

37 Q. Liu, J. Huang, X. Zhang, L. Cao, D. Yang, J. Kim and L. Feng, *ACS Sustainable Chem. Eng.*, 2020, **8**, 16091–16096.

38 T. Tang, W.-J. Jiang, S. Niu, N. Liu, H. Luo, Y.-Y. Chen, S.-F. Jin, F. Gao, L.-J. Wan and J.-S. Hu, *J. Am. Chem. Soc.*, 2017, **139**, 8320–8328.

39 G. Qian, J. Chen, T. Yu, L. Luo and S. Yin, *Nano Micro Lett.*, 2021, **13**, 77.

40 G. Qian, G. Yu, J. Lu, L. Luo, T. Wang, C. Zhang, R. Ku, S. Yin, W. Chen and S. Mu, *J. Mater. Chem. A*, 2020, **8**, 14545–14554.

41 T. Kou, S. Wang, R. Shi, T. Zhang, S. Chiovoloni, J. Q. Lu, W. Chen, M. A. Worsley, B. C. Wood, S. E. Baker, E. B. Duoss, R. Wu, C. Zhu and Y. Li, *Adv. Energy Mater.*, 2020, **10**, 2002955.

42 A. Qayum, X. Peng, J. Yuan, Y. Qu, J. Zhou, Z. Huang, H. Xia, Z. Liu, D. Q. Tan, P. K. Chu, F. Lu and L. Hu, *ACS Appl. Mater. Interfaces*, 2022, **14**, 27842–27853.

43 B. Liu, Y. Wang, H. Peng, R. Yang, Z. Jiang, X. Zhou, C. Lee, H. Zhao and W. Zhang, *Adv. Mater.*, 2018, **30**, 1803144.

44 X. Zou, Y. Wu, Y. Liu, D. Liu, W. Li, L. Gu, H. Liu, P. Wang, L. Sun and Y. Zhang, *Chem*, 2018, **4**, 1139–1152.

45 S. Yao, V. Forstner, P. W. Menezes, C. Panda, S. Mebs, E. M. Zolnhofer, M. E. Miehlich, T. Szilvási, N. Ashok Kumar, M. Haumann, K. Meyer, H. Grützmacher and M. Driess, *Chem. Sci.*, 2018, **9**, 8590–8597.

46 Y. Lyu, R. Wang, L. Tao, Y. Zou, H. Zhou, T. Liu, Y. Zhou, J. Huo, S. P. Jiang, J. Zheng and S. Wang, *Appl. Catal., B*, 2019, **248**, 277–285.

47 Y. Pan, S. Liu, K. Sun, X. Chen, B. Wang, K. Wu, X. Cao, W. Cheong, R. Shen, A. Han, Z. Chen, L. Zheng, J. Luo, Y. Lin, Y. Liu, D. Wang, Q. Peng, Q. Zhang, C. Chen and Y. Li, *Angew. Chem. Int. Ed.*, 2018, **57**, 8614–8618.

48 P. Guo, J. Wu, X.-B. Li, J. Luo, W.-M. Lau, H. Liu, X.-L. Sun and L.-M. Liu, *Nano Energy*, 2018, **47**, 96–104.

49 T. Liu, P. Li, N. Yao, T. Kong, G. Cheng, S. Chen and W. Luo, *Adv. Mater.*, 2019, **31**, 1806672.

50 H. Liu, J. Guan, S. Yang, Y. Yu, R. Shao, Z. Zhang, M. Dou, F. Wang and Q. Xu, *Adv. Mater.*, 2020, **32**, 2003649.

51 L. Ji, J. Wang, X. Teng, T. J. Meyer and Z. Chen, *ACS Catal.*, 2020, **10**, 412–419.

52 Y. Zhong, Y. Lu, Z. Pan, J. Yang, G. Du, J. Chen, Q. Zhang, H. Zhou, J. Wang, C. Wang and W. Li, *Adv. Funct. Mater.*, 2021, **31**, 2009853.

53 Z. Chen, Y. Ha, H. Jia, X. Yan, M. Chen, M. Liu and R. Wu, *Adv. Energy Mater.*, 2019, **9**, 1803918.

54 L. Dai, Z. Chen, L. Li, P. Yin, Z. Liu and H. Zhang, *Adv. Mater.*, 2020, **32**, 1906915.

55 D. Zhang, H. Mou, F. Lu, C. Song and D. Wang, *Appl. Catal., B*, 2019, **254**, 471–478.

56 H. Xu, B. Fei, G. Cai, Y. Ha, J. Liu, H. Jia, J. Zhang, M. Liu and R. Wu, *Adv. Energy Mater.*, 2020, **10**, 1902714.

57 Y. Xu, W. Tu, B. Zhang, S. Yin, Y. Huang, M. Kraft and R. Xu, *Adv. Mater.*, 2017, **29**, 1605957.

58 L. Yan, Y. Xu, P. Chen, S. Zhang, H. Jiang, L. Yang, Y. Wang, L. Zhang, J. Shen, X. Zhao and L. Wang, *Adv. Mater.*, 2020, **32**, 2070362.

59 G. Yilmaz, C. F. Tan, Y. Lim and G. W. Ho, *Adv. Energy Mater.*, 2019, **9**, 1802983.

60 J. Shi, F. Qiu, W. Yuan, M. Guo and Z.-H. Lu, *Chem. Eng. J.*, 2021, **403**, 126312.

61 P. W. Menezes, C. Panda, S. Garai, C. Walter, A. Guiet and M. Driess, *Angew. Chem. Int. Ed.*, 2018, **57**, 15237–15242.

62 F. Du, L. Shi, Y. Zhang, T. Li, J. Wang, G. Wen, A. Alsaedi, T. Hayat, Y. Zhou and Z. Zou, *Appl. Catal., B*, 2019, **253**, 246–252.